

Chemical order and size effects on the magnetic anisotropy of FePt and CoPt nanoparticles

Stanislas Rohart,^{1,2,*} Florent Tournus,¹ and Véronique Dupuis¹

¹*Université de Lyon, F-69000, France; Univ. Lyon 1, Laboratoire PMCN; CNRS, UMR 5586; F69622 Villeurbanne Cedex*

²*Laboratoire de Physique des Solides, CNRS, Université Paris Sud, UMR 8502, Bâtiment 510, F-91405 Orsay cedex, France*

(Dated:)

We investigate the consequence of the dimension reduction on the magnetic anisotropy of FePt and CoPt nanoparticles. Using an extension of the magnetic anisotropy model of Néel, we show that, due to a statistical finite size effect, chemically disordered clusters can display a magnetic anisotropy energy (MAE) as high as 0.5×10^6 J/m³, more than one order of magnitude higher than the bulk MAE. Concerning L1₀ ordered clusters, we show that the surface induces a reduction of the MAE as compared to the bulk, due to the symmetry breaking at the cluster surface, which modifies the chemical order.

PACS numbers: 75.75.+a, 75.30.Gw, 75.50.Bb, 75.50.Cc

I. INTRODUCTION

The understanding and the control of the nanostructure magnetic properties is a challenging field of research, for both fundamental and applied physics. At the nanoscale, finite size effects and surface contributions become dominant and lead to a modification of the properties as compared to the bulk, such as the enhancement of the orbital magnetic moment and of the magnetic anisotropy energy (MAE) at the less coordinated atoms.¹⁻⁴ However, technological applications of such structures for ultrahigh density magnetic storage media are limited by thermal fluctuations of the magnetization direction. To overcome this so-called superparamagnetic limit, intense efforts are devoted to the investigation of materials with a high MAE. In such a view FePt⁵⁻¹⁰ and CoPt¹¹⁻¹⁷ have become some of the most studied materials as they display a very large magnetocrystalline anisotropy (over 5×10^6 J/m³) when ordered in the L1₀ phase.

The effect of the L1₀ ordering in FePt and CoPt on the magnetic anisotropy in bulk crystals or thin films has been widely studied on both experimental and theoretical points of view.¹⁸⁻²² In the case of nanostructures, as the surface modifies the local chemical environment, it is expected to have potentially a large impact on the MAE. Although many experimental studies had been performed⁵⁻¹⁶, it is only recently that a clear impact of the dimension reduction on the MAE has been experimentally evidenced for CoPt nanoparticles.¹⁷ By using model samples, and combining various techniques, the authors have indeed been able to reliably determine the MAE of CoPt clusters with a diameter around 3 nm: while the anisotropy of chemically disordered particles was found to be higher than that of the bulk phase, it was the opposite for chemically ordered particles.

In this paper, we use an extension of the phenomenological anisotropy model of Néel to investigate the effect of chemical ordering and size reduction in both FePt and

CoPt clusters. We first show that this simple model is in good agreement with bulk and thin film results. Then, taking advantage of its simplicity, which allows us to perform an extensive study of FePt and CoPt nanoparticles, we use this model to investigate the MAE of clusters. Taking into account finite size effects by mean of a statistical analysis on a large number of nanostructures, we demonstrate the impact of L1₀ chemical ordering on the MAE and show how the surface and the finite size modify the results as compared to the bulk. Contrary to the results on pure Fe and Co clusters^{4,23}, here the surface induces a lowering of the MAE for L1₀ ordered clusters.

Using a simple phenomenological pair-interaction model to calculate an effect as subtle as the magnetic anisotropy may seem a quite hazardous approach as compared to more elaborate models, like ab-initio calculations. It is indeed well known that a theoretical determination of the MAE is a hard task: because it corresponds to very slight variations in the total energy as a function of the magnetization direction, highly converged results are required. Moreover, there is nowadays no available derivation of the Néel model from first principles. Nevertheless, this model, which is based on symmetries, has been found to be in good agreement with experiments on magnetic nanostructures^{4,23,24}. In particular it can remarkably well account for the prevailing effect of low-coordinated atoms on the MAE. This let us think that this empirical model must be valid to a certain point, and that it can give reliable tendencies regarding the evolution of the MAE in nanostructures with various parameters (size, shape, configuration...). Besides, let us note that a Néel expression for the local anisotropy is also used in atomic scale magnetic simulations based on a Heisenberg-type model.^{25,26} Unfortunately, even it can be quite successfully compared to some ab-initio calculations and experiments (see further in the paper), we cannot *demonstrate* the validity of the Néel model in the precise case under study: there is indeed no available ab-initio calculations of the MAE for comparable CoPt or

FePt nanoparticles. However, in order to study the effect of size reduction and of chemical ordering in particles of a few nanometers (which is precisely the size of interest for ultra-high density magnetic storage applications), there is no other method that can reasonably be used, and that would be more precise. We are then convinced that investigating such complex systems, which are out of reach for first-principle calculations for the moment, will give valuable physical insights. Knowing the results predicted by this simple and crude model will then enable further comparison with more advanced calculations in the future. It is also important to check if the predictions of the Néel model are correct in the case of alloy nanoparticles, and we hope that our work will stimulate experimental studies.

II. MAGNETIC ANISOTROPY OF A BIMETALLIC ALLOY

The magnetocrystalline anisotropy (MCA) arises from the coupling of the magnetization with the crystal lattice through the spin-orbit interaction²⁷. Then, for a given magnetic atom, it is directly linked to its local environment. For a whole structure, it is the signature of the system symmetries. It can be described using a phenomenological pair model, first introduced by L. Néel²⁸. In its original form, for a single element crystal, the MCA energy is written as a pair interaction over the first neighbors. The magnetic anisotropy energy of a dimer is expressed, using the lowest order term as²⁸

$$E_{\text{pair}} = -L(\mathbf{m} \cdot \mathbf{e})^2 \quad (1)$$

where \mathbf{m} is the magnetization unit vector and \mathbf{e} the unit vector along the bond. The prefactor L is the anisotropy parameter, which has to be determined and is generally fitted on bulk experiments.

To consider a given structure, we need two more hypothesis. First we suppose that the magnetization direction is homogeneous over the whole structure (macrospin approximation), which is a quite suitable approximation for nanostructures with dimensions close to the exchange length.²⁹ Second, we also suppose that the L parameter is the same in the bulk and at the cluster surface, and can be extracted from bulk measurements. Even if one could envisage a variation of the anisotropy parameter with the different environment in a structure, in fact the crude model of Néel with a uniform L extracted from bulk measurements has already shown a good agreement (qualitative at least but also quantitative) for such systems.^{4,23,24} As the purpose of our study is the prediction of the main tendencies, we will make this assumption in order to restrict the number of parameters in the model. On the basis of these two hypothesis, the total MCA energy, E_a , is evaluated by performing a sum over all the nearest neighbor pairs. This leads to a quadratic form, that can be diagonalized into the orthonormal basis set $(\mathbf{e}_1, \mathbf{e}_2, \mathbf{e}_3)$. The normalization condition on \mathbf{m}

further simplifies the expression to a biaxial form

$$E_a/V = -K_1(\mathbf{m} \cdot \mathbf{e}_1)^2 + K_2(\mathbf{m} \cdot \mathbf{e}_2)^2 + K \quad (2)$$

where V is the volume of the structure, K_1 and K_2 are positive constants and K a constant that can be omitted. Note that, in general cases, the new basis is different from the one defining the atomic lattice. The direction \mathbf{e}_1 (respectively \mathbf{e}_2) corresponds to the easy (respectively hard) magnetization direction, with the anisotropy constant K_1 (respectively K_2). This shows that this model, which is limited to second degree terms in \mathbf{m} , always leads to a biaxial second order magnetic anisotropy displaying two degenerated energy minima. At the equilibrium (at zero temperature), the magnetization lies along \mathbf{e}_1 and K_1V corresponds to the minimum energy needed to switch the magnetization from one minimum to the other one. Note that the value of K_2 does not influence this switching energy. For a bulk cubic crystal, this model would give a zero anisotropy, as the second order expression is not compatible with the cubic symmetry (for a more accurate description of the MCA in this case, one should use higher order terms in eq. 1, see ref. 24). However, this crude model is suitable to describe surface anisotropy where the cubic symmetry is locally broken.

To extend this model to an alloy containing two types of atom, named A and B in the following, three types of neighbor pair have to be considered:²² two between identical atoms and one between A and B atoms. We introduce three different anisotropy parameters: L_{AA} , L_{BB} and L_{AB} respectively for A - A , B - B and A - B pairs. The MCA energy is then evaluated by summing eq. 1 over all the nearest neighbors pairs, taking into account the chemical nature of the two atoms.

This model allows us to describe the effect of L1₀ chemical ordering on the MCA. Neglecting any tetragonal distortion, the atomic site lattice considered is face centered cubic (FCC), and we focus on equiatomic alloys. In this case, the L1₀ phase corresponds to an alternation of pure A and pure B planes in the [001] direction, leading to a chemical anisotropy along the c axis. Oppositely, in the chemically disordered phase named A1, the atoms are randomly distributed on the lattice sites. The magnitude of the chemical order is usually quantified by the long-range order (LRO) parameter S , which varies between 0 (totally disordered alloy) and 1 (perfectly ordered alloy)³⁰. Defining two sublattices labelled α and β , corresponding to successive planes in the [001] direction, S is given by

$$S = 2(n_\alpha - 1/2) \quad (3)$$

where n_α is the fraction of α sites occupied by atoms A . Note that changing the sign of S is equivalent to inverting the convention for the choice of the α and β planes. As this convention is arbitrary, the sign is meaningless and only the absolute value of S has to be considered. Conversely, the probability p for each lattice site to be occupied by an atom of the correct type (A in a α plane and B in a β plane) is directly related to S as $p = n_\alpha$.

To calculate the MCA of a bulk crystal of given order parameter, we consider the probability for a nearest neighbors pair to be a A - A , B - B or A - B bond and we calculate its average magnetic anisotropy parameter $\langle L \rangle$. Three different nearest neighbors pairs with equivalent $\langle L \rangle$ are obtained: those lying in the α planes, those lying in the β planes and those linking atoms from two different planes. The corresponding $\langle L \rangle$ parameters are respectively L_α , L_β , and $L_{\alpha\beta}$:

$$\begin{aligned} L_\alpha &= p^2 L_{AA} + (1-p)^2 L_{BB} + 2p(1-p) L_{AB} \\ L_\beta &= (1-p)^2 L_{AA} + p^2 L_{BB} + 2p(1-p) L_{AB} \\ L_{\alpha\beta} &= p(1-p) L_{AA} + p(1-p) L_{BB} + [p^2 + (1-p)^2] L_{AB}. \end{aligned}$$

For a chemically disordered crystal ($p = 1/2$), the probability to have a A or B atom on a given site is identical, and $L_\alpha = L_\beta = L_{\alpha\beta}$: the cubic symmetry is recovered and the MCA is zero. As soon as a chemical order arises in the crystal ($S > 0$), the cubic symmetry is broken and the second order MCA term has a finite value. Summing the different bond contributions in a FCC unit cell of volume V_{cell} , the MAE is obtained as

$$\begin{aligned} E_{a,\text{cell}} &= 2(L_\alpha + L_\beta - 2L_{\alpha\beta})(\mathbf{m} \cdot \mathbf{e}_c)^2 \\ &= 2(L_{AA} + L_{BB} - 2L_{AB})S^2(\mathbf{m} \cdot \mathbf{e}_c)^2, \quad (4) \end{aligned}$$

with \mathbf{e}_c the unit vector aligned along the c axis of the crystal. It corresponds to a uniaxial anisotropy, along the $[001]$ direction (c axis), and coincides with the chemical anisotropy direction. The anisotropy constant for the bulk alloy is then given by

$$K(S) = -2(L_{AA} + L_{BB} - 2L_{AB})S^2/V_{\text{cell}} \quad (5)$$

and has a simple quadratic form. This evolution can be understood looking back at our model: as a pair interaction is considered, the model involves products of the occupation probabilities for a given site, which are linear in S . If $2L_{AB} > L_{AA} + L_{BB}$, the anisotropy constant is positive, meaning that the c axis is the easy magnetization axis with the anisotropy constant $K_1 = K(S)$.

We now apply this model to the case of XPt crystals, where $X = \text{Fe}$ or Co . In these alloys, a strong second order MCA accompanies the chemical ordering into the $L1_0$ phase, and originates both from a local chemical environment change and from a tetragonal distortion of the FCC lattice. However, this slight deformation has a much weaker influence on the MCA²¹ and we neglect it in the following, as it was supposed in the previous development. In order to apply our model, we need to determine the parameters L_{XX} , L_{PtPt} and L_{XPt} . As the magnetic moment on the Pt atoms is small in these crystals^{8,18}, we neglect the magnetic anisotropy of the Pt-Pt bonds by taking $L_{\text{PtPt}} = 0$. A straightforward relation is then obtained between L_{XX} and L_{XPt} by fitting equation 5 on the experimental MAE value of the $L1_0$ ordered crystal. Consequently, there only remains one adjustable parameter and we finally estimate L_{XX} from measurements on pure samples using the original Néel model²³:

taking into account the magnetostriction parameters, the model gives $L_{XX}(r) = L_{XX}(r_0) + (r - r_0) \frac{dL_{XX}}{dr}(r_0)$, where r and r_0 are respectively the bond lengths in the alloy and in the pure crystal. We have determined the parameters for both FePt and CoPt (see table I). The L_{XX} parameter for $X = \text{Fe}$ and $X = \text{Co}$ has been calculated using the values given in ref.²³ and a bond length of respectively 2.72 Å for Fe and 2.71 Å for Co. In order to

XPt	K_{L1_0} (J/m ³)	L_{XX} (meV)	L_{XPt} (meV)
FePt	7.10 ⁶	0.23	0.73
CoPt	5.10 ⁶	0.91	0.89

TABLE I: Parameters L_{XX} and L_{XPt} of the Néel model for FePt and CoPt, determined as explained in the text from the $L1_0$ ordered bulk MAE and the bulk Fe and Co Néel model parameters²³.

check the accuracy of our model, we compare some predictions with bulk and thin film results. The variation of bulk FePt MAE versus S is compared to experiments³¹ and first principle calculations²¹, and, as it can be seen from fig. 1, shows a good agreement. The model is also compared to thin film experimental results. The MAE of a Pt/Co/Pt(111) multilayer with a Co thickness of one monolayer is

$$\frac{E_a}{\Sigma} = \frac{1}{s_{at}} \left(3L_{\text{CoPt}} - \frac{3}{2}L_{\text{CoCo}} \right) = 2K_S \quad (6)$$

where Σ is the film surface and s_{at}^{-1} is the surface atomic density. K_S is the usual surface anisotropy at the Co/Pt interface³² (the factor 2 on the right hand side of eq. 6 accounts for the two Co/Pt interfaces in the film). Using the values of table I, we find with our model $K_S = 1.17$ mJ/m², close to the value of 1.15 mJ/m² reported in ref³².

III. CHEMICAL ORDER IN NANOPARTICLES

In order to investigate the relationship between chemical order and magnetic anisotropy, we first need to precisely describe chemical order in nanostructures. Indeed, due to the finite size (and consequently the surface), the description is not as simple as in the bulk. First, the numbers of α and β sites are not necessarily equal like in the bulk. The order parameter has to be adapted, so that a particle with a perfect alternation of A and B planes displays $S = 1$. Using f_α the proportion of α sites, we use a more general definition of S :³⁰

$$S = \frac{n_\alpha - x}{1 - f_\alpha} \quad (7)$$

where n_α is, as before, the fraction of α sites occupied by a A atom, and x is the atomic concentration of A . Whereas for the bulk $f_\alpha = 1/2$ and eq. 3 is recovered, it

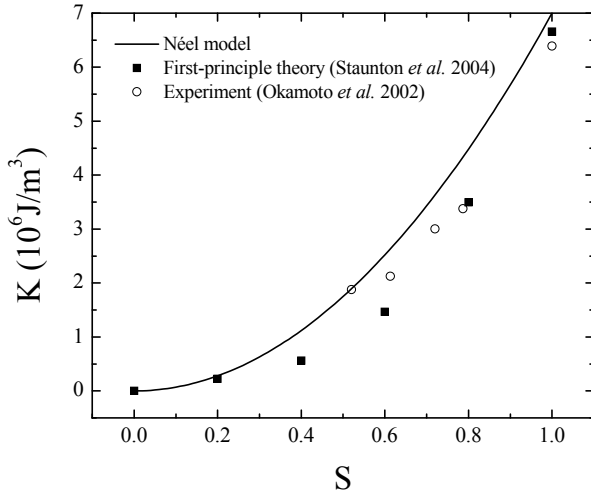


FIG. 1: Variation of the anisotropy constant K for a bulk FePt crystal versus the long-range chemical order parameter S . The results of our model (continuous line) are compared to experiments performed by S. Okamoto *et al.*³¹ and to first-principle calculations performed by J.B. Staunton *et al.*²¹

varies depending on the shape and the size of a nanoparticle. Moreover, note that inverting the convention for α and β planes changes f_α (for example, the truncated octahedron cluster, as the one represented in fig. 2, would display $f_\alpha = 0.507$ or 0.493 depending on the convention), but of course do not change the absolute value of S . Besides, a physical inversion of the atomic type on each lattice site will change S into $-S$, meaning that the physical chemical order is unchanged. However, in this case, the inversion leads to a cluster with a different stacking (in particular, the surface atoms are not the same) and possibly with different magnetic properties, as it will be discussed later.

To obtain a complementary description of the chemical order we can also use a short-range order (SRO) parameter, since for small size systems short-range ordering may dominate and control the nanoparticle properties. Although the SRO and LRO descriptions are equivalent for an infinite bulk (where there exists a direct relation between p , the probability for each site to be occupied by an atom of the correct type, SRO and LRO parameters³³) it is not true in nanoparticles. As our anisotropy model is limited to the first neighbors, we also limit the SRO parameter to the nearest neighbors and use the description of Cowley.³³ With $p_{l,m,n}$ the probability for an atom i on a given site to have, in the (l, m, n) direction, a nearest neighbor of the same kind, a local order parameter can be written as

$$a_{l,m,n} = 1 - \frac{1 - p_{l,m,n}}{x}$$

where x is, as before, the atomic concentration in A. In an infinite AB FCC crystal and for a given atom, 12 of these parameters can be calculated. However, regarding the $L1_0$ ordering, they are all equivalent (note that this

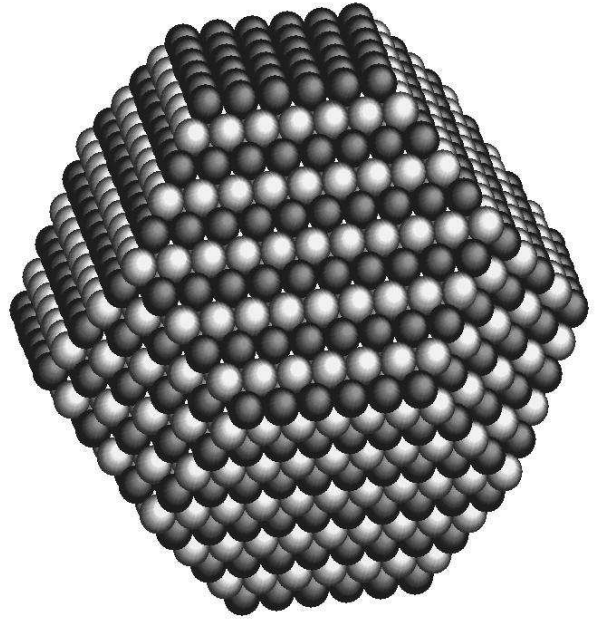


FIG. 2: Sketch of a $L1_0$ ordered truncated octahedron cluster containing 2406 atoms. The two colors represent the two types of atoms. Note that the topmost and bottommost planes contain the same kind of atom. Consequently, two types of cluster are possible: either the dark atoms correspond to A-type atoms, or they correspond to B-type atoms. These two clusters display different f_α factors, but have the same physical LRO parameter.

is not true for all types of order): $a_{l,m,n} = a_i$ for (l, m, n) directions in the (a, b) plane and $a_{l,m,n} = -a_i$ otherwise, with $a_i = 2p - 1$ if atom i is A-type on a α site or B-type on a β site and $a_i = 1 - 2p$ otherwise. One can then define the SRO parameter σ as the average of the a_i over the whole structure. Taking into account the occupation probability of each site, it leads to: $\sigma = (2p - 1)^2$.

This parameter is directly linked to the LRO parameter as $\sigma = S^2$. Note that this quadratic relation is understood by the fact that the LRO description is based on the lattice sites occupation whereas the SRO description is based on nearest-neighbor pair correlations.

In a nanoparticle, the SRO parameter has to be adapted due to the surface, as it was the case for S . For each atom i , we calculate a local order parameter σ_i as:

$$\sigma_i = \frac{n_i - x_i}{1 - f_i} \quad (8)$$

where n_i is the proportion of nearest-neighbors (NN) of the same chemical type as atom i , in the (\mathbf{a}, \mathbf{b}) plane, x_i is the proportion of NN of the same chemical type as atom i , among all its NN, and f_i is the proportion of NN in the (\mathbf{a}, \mathbf{b}) plane among all the NN (if atom i is surrounded by 12 NN like in the bulk, $f_i = 1/3$; if it is at a surface site, f_i may vary). The SRO parameter σ is then defined as the average of σ_i over the whole atoms. Of course, this definition of σ is identical to the Cowley-type one for the

infinite bulk.

An important feature, in the case of nanoparticles, is that the finite size allows us to explicitly take into account the statistical distribution of configurations. Indeed, the atomic arrangement for a given ordering probability p is not unique, resulting in a statistical distribution of the chemical order parameters S and σ . Then, the direct relation between S and p and the one between σ and S , established for an infinite system, are no more valid.

In order to investigate the relation between p , σ and S in nanoparticles, we have randomly generated a great number of nanoparticles with a given value of p . For each cluster, the true value of S and σ is calculated and we then obtain a statistical distribution of chemical order parameters (and of cluster composition), related to the small atom number in the cluster. Note that the choice of the direction defining the α and β sublattices is completely arbitrary, so that the [100] as well as the [010] or the [001] direction can be chosen to compute S and σ . In order to have a physical description of the chemical anisotropy, we always choose the directions that gives, on one hand the highest value of $|S|$, and on the other hand, the highest value of σ . For reasons explained further, we restrict our study to nanoparticles with a truncated octahedron shape.

We first focus on the chemical order in clusters where each site has an equal probability to be occupied by a A or B atom (i.e. $p = 1/2$). For each cluster, we have calculated both LRO and SRO parameters. Contrary to the bulk where a unique S and σ correspond to a given p , clusters display distributions of LRO and SRO, which are shown in fig. 3. As explained before, this is related to the small size of the particle and illustrates the distribution of configurations. This effect decreases when the diameter of the cluster increases, as the standard deviation of these parameters scales as the square root of the total number of atoms. Consequently, finite average values are found which means that the clusters cannot be considered as perfectly chemically disordered. The 201 atoms clusters display $\langle\sigma\rangle = 0.037$ and $\langle|S|\rangle = 0.094$ but note also that some clusters have a non-negligible probability to display chemical order parameter as high as $\sigma = 0.08$ or $|S| = 0.15$. Surprisingly, there is no detectable correlation between LRO and SRO for these clusters. This means that, for these disordered clusters, these parameters probe the chemical order in different and complementary ways and none of them is found to be better than the other one.

In partially ordered clusters ($p \neq 1/2$), the situation is quite different. Although a statistical distribution still exists, its width decreases with increasing p , which indicates that the number of configurations decreases. A clear correlation appear between LRO and SRO and their means follow the bulk relations: $\langle S \rangle \approx 2p - 1$ and $\langle \sigma \rangle \approx \langle S \rangle^2$.

In conclusion, we insist on the importance of the statistical distribution of configuration for nanoparticles.

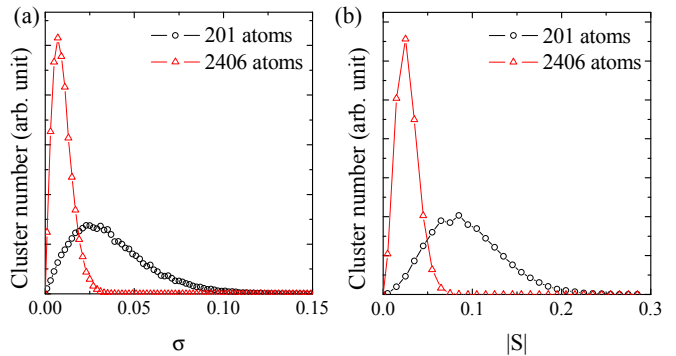


FIG. 3: Distribution of the SRO (σ) and LRO ($|S|$) parameters for disordered clusters containing 201 atoms (circles) and 2406 atoms (triangles).

Clusters generated with a given p present a distribution of chemical order parameters, and conversely, a variety of configurations correspond to clusters with the same order parameter. This means that, for small particles, chemical order parameters are not sufficient to fully characterize the chemical arrangement of atoms in the cluster: it is impossible to sum up an entire chemical configuration with only one or two numerical parameters. A statistical analysis is then essential to correctly investigate the link between chemical order and the physical properties in nanoparticles.

IV. MAGNETIC ANISOTROPY OF NANOPARTICLES

We now use this anisotropy model to investigate the consequence of the size reduction in FePt and CoPt nanoparticles, with respect to their chemical order. We focus on nearly spherical clusters, as it corresponds to the usual shape experimentally observed. Moreover, as the host lattice for the FePt and CoPt crystal is FCC, we have chosen to restrict our study to clusters with a perfect truncated octahedron (TO) shape (see figure 2), which is the equilibrium shape in this case^{6,34,35}. The magnetic anisotropy of pure Co TO clusters has already been studied using the Néel model²³. It has been shown that, due to the symmetries of the TO shape, both surface and volume MCA are zero (the MCA of the facets compensates) and that a surface anisotropy only arises when additional facets are present. Therefore, the MAE of perfect TO clusters, studied with our model will explicitly reveal the effects of size reduction and chemical ordering. Moreover, for the sake of simplicity, and in order to avoid any effect coming from the variation of the magnetic element concentration, we have only considered clusters with a composition around 50 % Pt. The dipolar interaction is also neglected in our study, since it is expected to play a significant role only for non-spherical clusters (shape anisotropy).³⁶

Concerning the magnetic anisotropy, whereas the bulk

FePt or CoPt MCA is only uniaxial, the cluster finite size implies that this is no more true and the more general biaxial form (see eq. 2) is always found. However, since the main point of interest is the minimum energy needed to switch the magnetization from an easy magnetization direction to the opposite one, we restrict our discussion to K_1 .

A. Chemically disordered nanoparticles

We first focus on the case of fully disordered clusters (*i.e.* when $p = 1/2$, each site having an equal probability to be occupied by a X or a Pt atom). For each cluster, we have calculated K_1 by summing eq. 1 over all the nearest neighbors bonds. We obtain a statistical distribution which is displayed on figure 4 for different types of clusters. Just like the S and σ distributions, the K_1 distribution is related to the small size of the cluster and its standard deviation scales as the square root of the total number of atoms in the cluster. Note also, that as for $|S|$ and σ , the mean value of K_1 decreases when the cluster size increases, indicating that for a large number of atoms

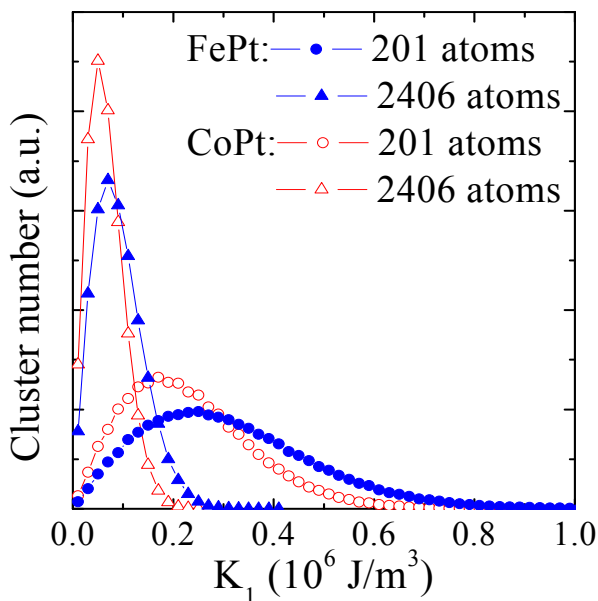


FIG. 4: Distribution of the magnetic anisotropy K_1 for FePt (close symbols) and CoPt (open symbols) disordered clusters containing 201 atoms - about 1.7 nm in diameter - (circles) and 2406 atoms - about 4.3 nm in diameter - (triangles).

Besides, we have observed that the $|S|$ and K_1 distributions are statistically independent which means that no detectable correlation exists between them. At first sight, this may seem surprising. In fact these two quantities are very different: S probes the long-range chemical order whereas K_1 is sensitive to the local chemical order around the magnetic atoms. A perfectly L1₀ ordered bulk structure with an antiphase boundary (*i.e.*

an inversion in the X and Pt planes stacking sequence) exemplifies this difference: whereas S will be zero, the magnetic anisotropy will almost be unaffected. A small S is then not incompatible with a significant MCA. Note however that a strong correlation exists between $|S|$ and K_1 when clusters display a higher chemical order, as it will be discussed later.

The local character of the magnetic anisotropy let us expect a stronger link between K_1 and the SRO parameter, because they both depend on NN correlations. Indeed, we obtain a noticeable correlation between K_1 and σ . However, although the correlation coefficient between K_1 and σ is significantly higher than the one between K_1 and S , and moreover increases with the particle size, it remains small. In particular, it corresponds to an insignificant variation of $\langle K_1 \rangle$ with σ , as compared to the K_1 statistical distribution (this can be seen in figure 7 for $\sigma \sim 0$). In small disordered particles, the configuration distribution is responsible for a partial “decorrelation” between the SRO and the magnetic anisotropy. Although the SRO parameter is more suited than the LRO one, it still fails to establish a definite link between chemical order and magnetic anisotropy.

We have also investigated the spatial distribution of the cluster easy magnetization axis direction (\mathbf{e}_1 vector). Whereas the L1₀ ordering induces an anisotropy axis along the c axis, we do not find such a result for disordered clusters. The \mathbf{e}_1 direction distribution satisfies the cluster cubic symmetry and the three a , b and c axes are found to be equivalent. However, the distribution is inhomogeneous and a probability maximum occurs in the [110] direction (and the other equivalent directions), as shown in fig. 5. This means that the easy magnetization axis is rarely oriented towards the {001} or {111} facets of the TO cluster but generally points towards the edges connecting two {111} faces. Moreover, this direction also corresponds to a maximum of the MAE: in the case of the 201 atom FePt cluster presented in fig. 5, the mean MAE is about 0.35×10^6 J/m³ for an easy axis aligned along the [110] direction while it is about 0.20 and 0.25×10^6 J/m³ respectively in the [001] and [111] directions.

B. Chemical ordering

To study the chemical ordering effect in nanoparticles, clusters with different p values were generated, leading in each case to a finite width distribution for $|S|$ and σ (except for $p = 1$). In this way, a large number of configurations is obtained allowing us to investigate the relation between $|S|$, σ and K_1 . The results are represented in fig. 6 and 7 revealing the statistical nature of the link between S , σ and K_1 . These Figures are analogous to the bulk $K(S)$ curve but also shows the finite width distributions.

Although in the bulk, simple relations have been found between K_1 and S (quadratic variation) or σ (linear vari-

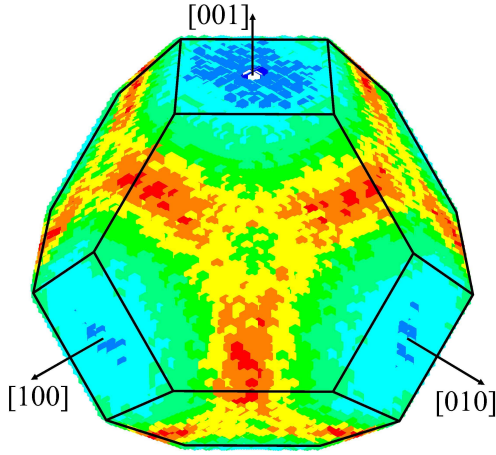


FIG. 5: (color online) Statistical distribution of the easy magnetization axis for a 201 atom FePt cluster, represented in a 3D view along the $[111]$ direction. The color scale represents the probability density for the easy magnetization axis to point in the corresponding direction, red (resp. blue) areas indicating the most (less) probable directions.

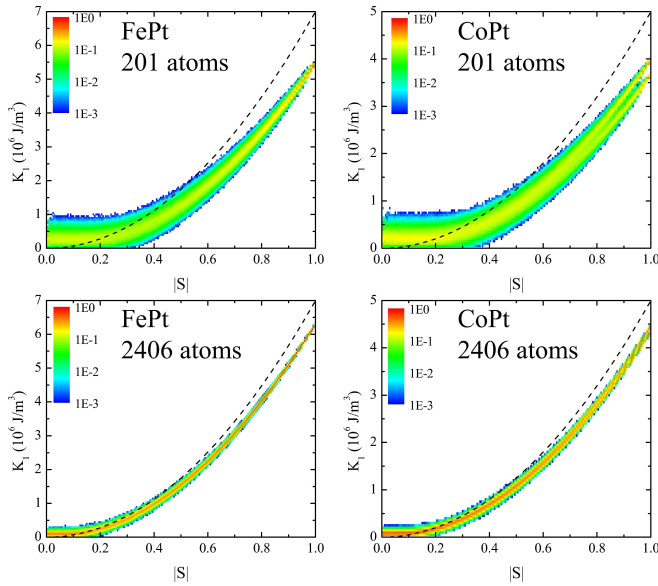


FIG. 6: (color online) Variation of the anisotropy constant K_1 versus $|S|$ for a 201 atoms FePt (a) and CoPt (b) cluster, and for a 2406 atoms FePt (c) and CoPt (d) cluster. The color scale represents in the $(|S|, K_1)$ plane, the density of probability for a cluster with chemical long range order parameter $|S|$ to have a MCA K_1 (the corresponding color bar is shown in inset). The dashed line corresponds to the bulk behavior.

ation), the relation is more complex for clusters. For small $|S|$ or σ , the mean K_1 is higher than the one of the bulk and we find the result previously described: versus S , the K_1 distribution is constant (mean value and width) and versus σ , a very small increase of the mean K_1 occurs. In this case, the magnetic anisotropy is dominated by the small size effect, in particular by the statis-

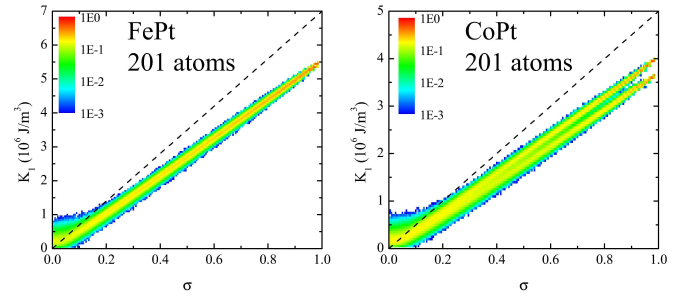


FIG. 7: (color online) Variation of the anisotropy constant K_1 versus σ for a 201 atoms FePt (a) and CoPt (b) cluster. The color scale represents in the (σ, K_1) plane, the density of probability for a cluster with chemical short range order parameter $|\sigma|$ to have a MCA K_1 (the corresponding color bar is shown in inset). The dashed line corresponds to the bulk behavior.

tical distribution of the atoms on the lattice sites. Above a threshold (S_{th} or σ_{th} respectively for LRO and SRO parameters), $\langle K_1 \rangle$ starts increasing and the distribution narrows (note that the threshold is the same for the two order parameters as $\sigma_{th} = S_{th}^2$). $\langle K_1 \rangle$ is proportional to $|S|^2$ or to σ , similarly to the bulk, which means that the chemical order is sufficient to induce a significant effect on the MAE. However, the increase is smaller than for the bulk and the perfectly ordered $L1_0$ cluster magnetic anisotropy appears to be weaker than for the bulk. As it will be discussed later, this is due to a surface effect. The case of CoPt clusters is even more complex, as the magnetic anisotropy displays two distinct limits for perfectly ordered clusters. The difference is $0.32 \times 10^6 \text{ J/m}^3$ for the 201 atoms CoPt clusters. This corresponds to two different $L1_0$ ordered clusters where the Co and Pt atoms have been exchanged. As previously discussed in section III this does not change the order parameter but, while in one case the top and bottom facets are made of Co atoms, in the other case they are made of Pt atoms, the magnetic properties are different (the MAE is higher in this case). This effect also exists for FePt clusters but is weaker (the energy difference is only $0.2 \times 10^4 \text{ J/m}^3$) and it is not visible on the figures. Finally, as the cluster size increases, the threshold decreases and the K_1 value for $L1_0$ ordered clusters increases, meaning that the behavior is getting closer to the bulk one.

Our calculations have also revealed that, as the chemical order increases, the easy magnetization direction gets closer to the c axis. When p is high enough (which corresponds to $|S|$ above the threshold mentioned earlier), the easy axis is contained in a cone around the c axis whose summit angle decreases as p increases, as shown in figure 8.

As a matter of fact, our results do not show any particular difference between the description using a SRO or a LRO parameter. In fact, as long as the chemical order is significant, a coherence is developed over the whole particle (statistically, a significant LRO goes with a sig-

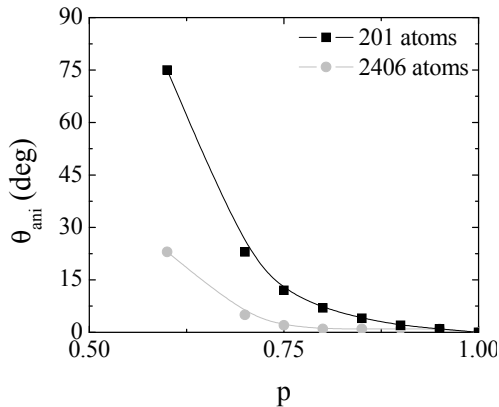


FIG. 8: Variation of the anisotropy cone angle θ_{ani} (summit half angle) versus p for 201 and 2406 FePt atoms clusters. The anisotropy cone is defined as the one, around the c axis, containing 90% of the easy magnetization axes.

nificant SRO) and both parameters are highly correlated with the magnetic anisotropy. The SRO description is found to be slightly more convenient only for disordered clusters. On the other hand, the theoretical variation of the magnetic anisotropy with the LRO parameter may be more useful for comparisons with experiments, or with more advanced calculations,^{5,9,10,19,21} since the LRO parameter is usually used to quantify the degree of order in CoPt and FePt alloys. Moreover, while there is to our knowledge no reported experimental measurement of a SRO parameter, for CoPt or FePt nanoparticles as those considered in our study, it is possible to determine their individual (using for instance transmission electron microscopy) or their mean LRO parameter.^{37–40}

V. DISCUSSION

To apprehend the joint effects of surface and of small size in XPt clusters ($X = \text{Co, Fe}$), we focus on two extreme cases: fully disordered and perfectly $L1_0$ ordered clusters. These systems show a completely different variation of the MCA versus the cluster size, as it can be seen in figure 9. In the limit of large diameters, bulk results are recovered: disordered clusters have a zero MCA and $L1_0$ ordered clusters display MCA of 7 and $5 \times 10^6 \text{ J/m}^3$, respectively for FePt and CoPt. For a finite diameter, chemically disordered (resp. $L1_0$ ordered) clusters display a higher (resp. lower) MCA than the bulk one.

For perfectly ordered clusters ($S = 1$), the variation of $\langle K_1 \rangle$ versus the number N of atoms in a cluster can be adjusted by this expression

$$\langle K_1 \rangle (N) = K_V + \frac{K_a}{N^{1/3}} \quad (9)$$

where K_V is the bulk MAE, at the corresponding S , and the second term is a small size correction. This small

size correction can be read in terms of a surface magnetic anisotropy because it scales with the surface to volume ratio Σ/V . It could be alternatively written as $K_S \Sigma/V$, with K_S the surface magnetic anisotropy. Accordingly, the total anisotropy energy for a particle can then be written, in an usual way, as the sum of a volume and a surface contribution: $E_a = K_V V + K_S \Sigma$. However, in the present case K_S is negative, which is very unusual. The negative sign of K_S indicates a lowering of the MCA at the smallest sizes, as the chemical order is broken at the surface: due to missing neighbors, the contribution of the XPt bonds is reduced and the total MCA decreases. We find $K_S = -0.42$ and -0.33 mJ/m^2 for the FePt clusters, and -0.32 and -0.23 mJ/m^2 for the CoPt clusters. For each type of clusters, two values for K_a (and thus for K_S) are found due to the non-equivalence between the two $L1_0$ stacking possibilities, which indicates that the surface effects depend on the type of facets: the clusters which have the highest anisotropy have pure Pt upper and lower $[001]$ facets. This small size effect cannot be neglected for the smallest clusters: for less than 2000 atoms (about 3.5 nm in diameter), the decrease is more than 10 % as compared to the bulk. It is worth to mention that the absolute value of this surface magnetic anisotropy is comparable to the highest one reported for pure clusters embedded in various matrices^{41–43}.

For chemically disordered clusters ($S = 0$) equation 9 cannot be used to account for the variation of $\langle K_1 \rangle$ with N . Interestingly, in this case the evolution corresponds to the expression

$$\langle K_1 \rangle (N) = K_V + \frac{K_b}{N^{1/2}} \quad (10)$$

indicating that in this case, the small size contribution does not originate from a surface effect. Here, the effect scales with the inverse square root of the number of atoms, which is reminiscent of a statistical effect. Indeed, as discussed before, for small disordered clusters the statistical distribution of the various chemical configurations is responsible for a concomitant (but uncorrelated) enhancement of the mean long range order parameter and of the mean anisotropy constant.

In the case of intermediate S values, the evolution of $\langle K_1 \rangle$ can be adjusted by a combination of the two preceeding expressions:

$$\langle K_1 \rangle (N) = K_V + \frac{K_a}{N^{1/2}} + \frac{K_b}{N^{1/3}}, \quad (11)$$

where the two constants K_a and K_b respectively account for the statistical/configuration effect and the surface effect. The results of the fits are shown in table II for different values of $|S|$, both for FePt and CoPt clusters. The relative weight of these two contributions gives us information on the origin of the anisotropy variation with size. We find that the magnitude of the surface contribution (i.e. the absolute value of K_b) increases with the

chemical order parameter of the particles, while the behavior of the statistical contribution is less intuitive: K_a is first increasing with S and then finally vanishes when S reaches 1. Note also that, since the surface and the configuration contributions to the MAE have opposite signs, there exists a range of S values where there is almost no evolution of $\langle K_1 \rangle$ with the particle size.

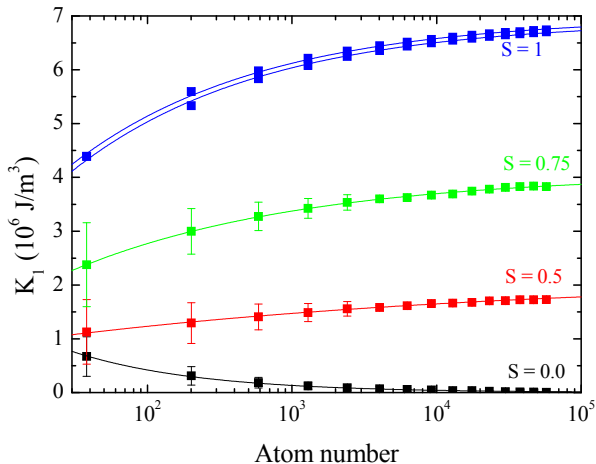


FIG. 9: Variation of the mean anisotropy constant $\langle K_1 \rangle$ versus the number of atoms in the cluster for FePt clusters of different $|S|$ parameters. The dots correspond to the calculated $\langle K_1 \rangle$, the error bar representing the FWHM of the K_1 distributions. The lines are obtained by fitting the calculated values with the expression proposed in the text.

$ S $	FePt			CoPt		
	K_V	K_a	K_b	K_V	K_a	K_b
0	0.0	4.2	0.0	0.0	3.0	0.0
0.5	1.9	6.4	-5.9	1.3	4.0	-3.8
0.75	4.0	3.6	-7.4	2.8	3.1	-5.0
1	7.0	0.0	-9.2/-8.5	5.0	0.0	-6.9/-5.1

TABLE II: Volume anisotropy K_V and small size correction coefficients K_a and K_b , determined for several S using eq. 11, from the results in fig 9. The two different values of K_b for $L1_0$ ordered clusters account for the two types of $L1_0$ stacking as discussed previously. Magnetic anisotropies are given in 10^6 J/m^3 .

The predictions of the empirical Néel model can be of great help to analyze experimental magnetic measurements. Indeed, according to the present results, we can expect the chemically disordered particles to have a quite high anisotropy (much higher than that of the bulk phase), whereas it should be in fact impossible to obtain small chemically ordered nanoparticles having an intrinsic MCA as high as that of the bulk $L1_0$ phase. This is consistent with our very recent experimental findings on CoPt nanoparticles.¹⁷ In addition, our calculations show that the anisotropy constant is falling off rapidly when a particle is not fully ordered, which could also be responsible of the experimental observation of a lower MAE than

expected. This point may be particularly relevant, since it is predicted that the most favorable configurations for small particles correspond to $S < 1$.⁴⁴ We emphasize that the results reported in this paper have been obtained by completely letting aside any energetic consideration for the various chemical arrangements. Nevertheless, our model could easily be combined with a structural optimization method, either to determine the MAE of a few particular structures predicted to be the most stable ones, or to determine the MAE distribution of a statistical ensemble of structures, taking into account their probability of existence.

Another interesting feature predicted by our model is the significant MAE distribution, even for a given particle size and a fixed chemical order parameter, which is due to the existence of a statistical set of chemical configurations. As discussed elsewhere,⁴⁵ this can be one of the major source of MAE distribution in realistic assemblies of clusters (with a distribution of composition, size, shape...). This feature, which is a particularity of magnetic alloys, should be directly visible in experimental measurements on well-defined samples.

VI. CONCLUSION

In this study, we have extended the anisotropy model of Néel²⁸ to describe the magnetocrystalline anisotropy in mixed FePt and CoPt crystals. This phenomenological model allows us to describe the effect of $L1_0$ ordering on the MCA and appears to be in good agreement with previously reported results on bulk and thin films. We have used this model to investigate the specific modifications occurring in nanosized clusters of FePt and CoPt with a truncated octahedron shape. In chemically disordered clusters, we have shown that there always exists a partial chemical order, due to the small number of atoms, and that, oppositely to the bulk, the MCA is non zero. On the contrary, for $L1_0$ ordered clusters, we have shown that surface induces a strong diminution of the magnetic anisotropy, due to the broken $L1_0$ periodicity at the cluster surface.

Our finding points a lack in this type of ordered alloys as materials for high-density magnetic storage applications, where a high switching energy $K_{\text{eff}}V$ is needed to stabilize the magnetization direction. In pure or chemically disordered clusters, the anisotropy constant increases when the size decreases, thanks to a positive surface MAE (see e.g. ref. 3,4,43), which attenuates the size variation of the switching energy. On the contrary, in the $L1_0$ ordered CoPt and FePt clusters, K_{eff} decreases when the size decreases due to the negative surface MAE, which worsens the size variation of the switching energy. Here, surface is a drawback that may be compensated by playing on appropriate surface effects. Changing the surface anisotropy sign could be achieved using the high interface magnetic anisotropy that adds to surface magnetic anisotropy when the cluster surface is in contact

with an appropriate non ferromagnetic material, like Pt⁴² or CoO⁴⁶. Surface engineering, by embedding the clusters in the matrix or by synthesizing core-shell clusters with the non ferromagnetic shell around the magnetic core, appears to be complementary approaches to these L1₀ ordered materials, in order to overcome the superparamagnetic limit in nanoscale clusters.

Acknowledgments

We gratefully acknowledge V. Repain and Y. Nahas (MPQ, Paris, France) for stimulating discussions. We acknowledge support from the European Community (STREP SFINx no. NMP2-CT-2003-505587).

-
- * Electronic address: rohart@lps.u-psud.fr
- ¹ P. Gambardella, S. Rusponi, M. Veronese, S. S. Dehsi, C. Grazioli, A. Dallmeyer, I. Cabria, R. Zeller, P. H. Dedrichs, K. Kern, C. Carbone, and H. Brune, *Science* **300**, 1130 (2003).
 - ² I. M. Billas, A. Châtelain, and W. A. de Heer, *Science* **265**, 1682 (1994).
 - ³ S. Rusponi, T. Cren, N. Weiss, M. Epple, P. Bulushek, L. Claude, and H. Brune, *Nature Mater.* **2**, 546 (2003).
 - ⁴ M. Jamet, W. Wernsdorfer, C. Thirion, D. Mailly, V. Dupuis, P. Mélinon, and A. Pérez, *Phys. Rev. Lett.* **86**, 4676 (2001).
 - ⁵ S. Sun, C. B. Murray, D. Weller, L. Folks, and A. Moser, *Science* **287**, 1989 (2000).
 - ⁶ Z. R. Dai, S. Sun, and Z. L. Wang, *Nano Letters* **1**, 443 (2001).
 - ⁷ B. Rellinghaus, S. Stappert, M. Acet, and E. F. Wassermann, *J. Magn. Magn. Mat.* **266**, 142 (2003).
 - ⁸ C. Antoniak, J. Lindner, M. Spasova, D. Sudfeld, M. Acet, M. Farle, K. Fauth, U. Wiedwald, H.-G. Boyen, P. Ziemann, F. Wilhelm, A. Rogalev, and S. Sun, *Phys. Rev. Lett.* **97**, 117201 (2006).
 - ⁹ C. Rong, D. Li, V. Nandwana, N. Poudyal, Y. Ding, Z. L. Wang, H. Zeng, and J. Ping Liu, *Adv. Mater.* **18**, 2984 (2006).
 - ¹⁰ C. Rong, N. Poudyal, G. S. Chaubey, V. Nandwana, R. Skomski, Y. Q. Wu, M. J. Kramer, and J. Ping Liu, *J. Appl. Phys.* **102**, 43913 (2007).
 - ¹¹ A. C. C. Yu, M. Mizuno, Y. Sasaki, H. Kondo, and K. Hiraga, *Appl. Phys. Lett.* **81**, 3768 (2002).
 - ¹² Y. Xu, Z. G. Sun, Y. Qiang, and D. J. Sellmyer, *J. Magn. Magn. Mat.* **266**, 164 (2003).
 - ¹³ C. Petit, S. Rusponi, and H. Brune, *J. Appl. Phys.* **95**, 4251 (2004).
 - ¹⁴ X. Sun, Z. Y. Jia, Y. H. Huang, J. W. Harrell, D. E. Nikles, K. Sun, and L. M. Wang, *J. Appl. Phys.* **95**, 6747 (2004).
 - ¹⁵ M. Mizuno, Y. Sasaki, M. Inoue, C. N. Chinnaamy, B. Jeyadevan, D. Hasegawa, T. Ogawa, M. Takahashi, K. Tohji, K. Sato, and S. Hisano, *J. Appl. Phys.* **97**, 10J301 (2005).
 - ¹⁶ L. Castaldi, K. Giannakopoulos, A. Travlos, D. Niarchos, S. Boukari, and E. Beaurepaire, *J. Magn. Magn. Mat.* **290-291**, 544 (2005).
 - ¹⁷ F. Tournus, A. Tamion, N. Blanc, A. Hannour, L. Bardotti, B. Prével, P. Ohresser, E. Bonet, T. Epicier, and V. Dupuis, *Phys. Rev. B* **77**, 144411 (2008).
 - ¹⁸ W. Grange, I. Galanakis, M. Alouani, M. Maret, J. P. Kappler, and A. Rogalev, *Phys. Rev. B* **62**, 1157 (2000).
 - ¹⁹ S. A. Razee, J. B. Staunton, B. Ginatempo, E. Bruno, and F. J. Pinski, *Phys. Rev. B* **64**, 014411 (2001).
 - ²⁰ O. Ersen, V. Parasote, V. Pierron-Bohnes, M. C. Cadeville, and C. Ulhaq-Bouillet, *J. Appl. Phys.* **93**, 2987 (2003).
 - ²¹ J. B. Staunton, S. Ostanin, S. S. A. Razee, B. Gyorffy, L. Szunyogh, B. Ginatempo, and E. Bruno, *J. Phys. Cond. Matt.* **16**, S5623 (2004).
 - ²² R. Skomski, *J. Appl. Phys.* **101**, 9N517 (2007).
 - ²³ M. Jamet, W. Wernsdorfer, C. Thirion, V. Dupuis, P. Mélinon, A. Pérez, and D. Mailly, *Phys. Rev. B* **69**, 024401 (2004).
 - ²⁴ R. Morel, A. Brenac, C. Portemont, T. Deutsch, and L. Notin, *J. Magn. Magn. Mat.* **308**, 296 (2007).
 - ²⁵ D. A. Garanin, and H. Kachkachi, *Phys. Rev. Lett.* **90**, 065504 (2003); H. Kachkachi, and E. Bonet, *Phys. Rev. B* **73**, 224402 (2006).
 - ²⁶ T. Jourdan, F. Lançon, and A. Marty, *Phys. Rev. B* **75**, 094422 (2007).
 - ²⁷ P. Bruno, *Phys. Rev. B* **39**, 865 (1989).
 - ²⁸ L. Néel, *J. Phys. Radium* **15**, 225 (1954).
 - ²⁹ A. Hubert and R. Schäfer, *Magnetic domains* (Springer, Berlin, 1998).
 - ³⁰ F. C. Nix and W. Shockley, *Rev. Mod. Phys.* **10**, 1 (1938).
 - ³¹ S. Okamoto, N. Kikuchi, O. Kitakami, T. Miyazaki, Y. Shimada, and K. Fukamichi, *Phys. Rev. B* **66**, 024413 (2002).
 - ³² N. McGee, M. Johnson, J. de Vries, and J. A. de Stegee, *J. Appl. Phys.* **73**, 3418 (1993).
 - ³³ J. M. Cowley, *J. Appl. Phys.* **21**, 24 (1950).
 - ³⁴ R. van Hardeveld and F. Hartog, *Surf. Sci.* **15**, 189 (1969).
 - ³⁵ L. Favre, V. Dupuis, E. Bernstein, P. Melinon, A. Perez, S. Stanesco, T. Epicier, J.-P. Simon, D. Babonneau, J.-M. Tonnerre, and J.-L. Hodeau, *Phys. Rev. B* **74**, 014439 (2006).
 - ³⁶ We have checked this point by explicitly calculating the shape anisotropy. Indeed, because we are dealing with alloys, even the highly symmetric truncated octahedron shape does not give zero dipolar anisotropy (shape anisotropy), but according to our calculations it remains negligible.
 - ³⁷ S. Stappert, B. Rellinghaus, M. Acet, and E. F. Wassermann, *J. Cryst. Growth* **252**, 440 (2003).
 - ³⁸ K. Sato, Y. Hirotsu, H. Mori, Z. Wang, and T. Hirayama, *J. Appl. Phys.* **98**, 024308 (2005).
 - ³⁹ R. V. Petrova, R. R. Vanfleet, D. R. Richardson, B. Yao, and K. R. Coffey, *IEEE Trans. Magn.* **41**, 3202 (2005).
 - ⁴⁰ S. Saita and S. Maenosono, *J. Phys. Cond. Matt.* **16**, 6385 (2004).
 - ⁴¹ M. Jamet, V. Dupuis, P. Melinon, G. Guiraud, A. Perez, W. Wernsdorfer, A. Traverse, and B. Baguenard, *Phys. Rev. B* **62**, 493 (2000).
 - ⁴² M. Jamet, M. Négrier, V. Dupuis, J. Tuillon-Combes, P. Melinon, A. Perez, W. Wernsdorfer, B. Barbara, and B. Baguenard, *J. Mag. Mag. Mat.* **237**, 293 (2001).
 - ⁴³ S. Rohart, C. Raufast, L. Favre, E. Bernstein, E. Bonet, and V. Dupuis, *Phys. Rev. B* **74**, 104408 (2006).

- ⁴⁴ M. Muller, P. Erhart, and K. Albe, Phys. Rev. B **76**, 155412 (2007).
- ⁴⁵ F. Tournus, S. Rohart, and V. Dupuis, IEEE Trans. Magn., in press.
- ⁴⁶ V. Skumryev, S. Stoyanov, Y. Zhang, G. Hadjipanayis, D. Givord, and J. Nogués, Nature **423**, 850 (2003).